Available online at www.sciencedirect.com
SCIENCE DIRECT®
Journal of Solid State Chemistry 178 (2005) 2313–2321
JOURNAL OF SOLID STATE CHEMISTRY
www.elsevier.com/locate/jssc

Structural analysis and characterization of layer perovskite oxynitrides made from Dion–Jacobson oxide precursors

Joshua A. Schottenfeld[a], Alan J. Benesi[a], Peter W. Stephens[b], Gugang Chen[c], Peter C. Eklund[c], Thomas E. Mallouk[a,*]

[a]*Department of Chemistry, The Pennsylvania State University, University Park, PA 16802, USA*
[b]*Department of Physics & Astronomy, State University of New York, Stony Brook, New York 11794, USA*
[c]*Departments of Physics, The Pennsylvania State University, University Park, PA 16802, USA*

Received 3 March 2005; received in revised form 9 May 2005; accepted 12 May 2005

Abstract

A three-layer oxynitride Ruddlesden–Popper phase $Rb_{1+x}Ca_2Nb_3O_{10-x}N_x \cdot yH_2O$ ($x = 0.7-0.8$, $y = 0.4-0.6$) was synthesized by ammonialysis at 800 °C from the Dion–Jacobson phase $RbCa_2Nb_3O_{10}$ in the presence of Rb_2CO_3. Incorporation of nitrogen into the layer perovskite structure was confirmed by XPS, combustion analysis, and MAS NMR. The water content was determined by thermal gravimetric analysis and the rubidium content by ICP-MS. A similar layered perovskite interconversion occurred in the two-layer Dion–Jacobson oxide $RbLaNb_2O_7$ to yield $Rb_{1+x}LaNb_2O_{7-x}N_x \cdot yH_2O$ ($x = 0.7-0.8$, $y = 0.5-1.0$). Both compounds were air- and moisture-sensitive, with rapid loss of nitrogen by oxidation and hydrolysis reactions. The structure of the three-layer oxynitride $Rb_{1.7}Ca_2Nb_3O_{9.3}N_{0.7} \cdot 0.5H_2O$ was solved in space group $P4/mmm$ with $a = 3.887(3)$ and $c = 18.65(1)$ Å, by Rietveld refinement of X-ray powder diffraction data. The two-layer oxynitride structure $Rb_{1.8}LaNb_2O_{6.3}N_{0.7} \cdot 1.0H_2O$ was also determined in space group $P4/mmm$ with $a = 3.934(2)$ and $c = 14.697(2)$ Å. GSAS refinement of synchrotron X-ray powder diffraction data showed that the water molecules were intercalated between a double layer of Rb+ ions in both the two- and three-layer Ruddlesden–Popper structures. Optical band gaps were measured by diffuse reflectance UV-vis for both materials. An indirect band gap of 2.51 eV and a direct band gap of 2.99 eV were found for the three-layer compound, while an indirect band gap of 2.29 eV and a direct band gap of 2.84 eV were measured for the two-layer compound. Photocatalytic activity tests of the three-layer compound under 380 nm pass filtered light with $AgNO_3$ as a sacrificial electron acceptor gave a quantum yield of 0.025% for oxygen evolution.

Keywords: Oxynitride; Perovskite; Photocatalysis

1. Introduction

The perovskite family of structures has been studied extensively because of the broad range of technologically important properties of perovskite oxides, oxynitrides, and fluorides. The oxides have been shown to be superconductors [1,2], ferroelectrics [3], colossal magnetoresistors [4], and catalysts [5–7]. The perovskite structural family can support a large number of elements, both on the cation and anion sites, which leads to tunability in these properties. Additionally, intergrowth structures in the perovskite family can be easily converted from one form to another [8–11]. Many of these conversions occur through "soft" chemistry, such as ion exchange and dehydration. One example of this is the conversion of a Dion–Jacobson phase ($A'A_{n-1}B_nO_{3n+1}$) [12–14] to Ruddlesden–Popper phase ($A'_2A_{n-1}B_nO_{3n+1}$) [15,16] by reduction of the *B*-site cation in rubidium vapor [17]. These techniques are very versatile and can be used to synthesize compositions not attainable by other means.

*Corresponding author. fax: +1 814 863 8403.
E-mail address: tom@chem.psu.edu (T.E. Mallouk).

0022-4596/$ - see front matter © 2005 Published by Elsevier Inc.
doi:10.1016/j.jssc.2005.05.012

Perovskite-structure oxides have been found to be good photocatalysts for overall water splitting. The quantum yields (QY) for water photolysis with $SrTiO_3$ [5,6] and $NaTaO_3$ [18] are higher than those obtained with binary oxide photocatalysts such as TiO_2 [19]. Layer perovskites are particularly good photocatalysts [20,21], presumably due to intercalation of water into the interlayer space. The ease with which their compositions can be varied, and the possibility of selectively modifying the interlayer space with hydrogen- or oxygen-evolving co-catalysts, also makes them attractive materials to explore [22]. Although these compounds are good ultraviolet (UV) water splitting photocatalysts, their large band gaps (>3 eV) preclude significant photoactivity in the visible part of the spectrum.

Nitrogen can be substituted for oxygen in three-dimensionally bonded perovskite structures by thermal reaction with ammonia [23–27]. The resulting oxynitrides have smaller band gaps than oxides of similar composition because of the relatively high energy of the nitrogen 2*p* states that make up the top of the valence band [28–30]. Titanate, niobate, and tantalate oxynitrides typically have bandgaps in the visible region of the spectrum. Ammonialysis to replace lattice oxygen by nitrogen in a layered perovskite Dion–Jacobson phase is possible, but charge balance requires an additional $+1$ charge in the lattice for every O^{2-} ion that is replaced by N^{3-}. Because compounds in the Ruddlesden–Popper series of layered perovskites contain twice as many interlayer cations as those in the Dion–Jacobson series, it should be possible to achieve the necessary charge balance by converting a Dion–Jacobson phase to a Ruddlesden–Popper phase. This idea is illustrated in Fig. 1. This reaction scheme, if successful, would add another transformation to the tool box of perovskite chemistry, in which it is possible to interconvert layer perovskites in the Dion–Jacobson, Ruddlesden–Popper, and Aurivillius families, often through "soft" topochemical reactions [11].

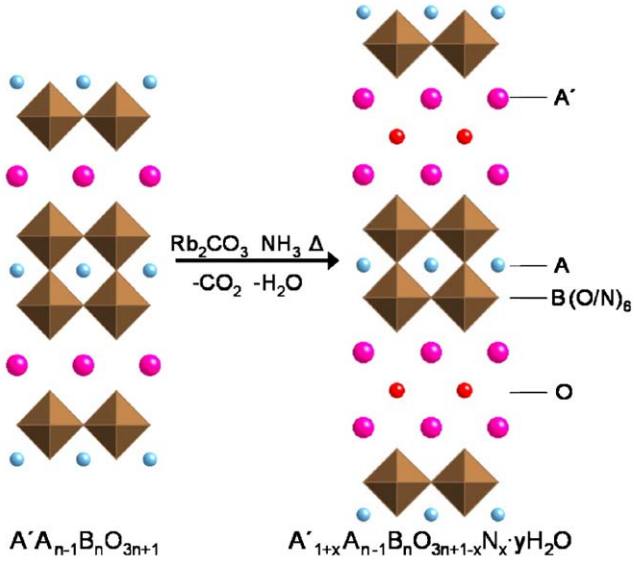

Fig. 1. Synthetic scheme for conversion of a Dion–Jacobson oxide to the corresponding Ruddlesden–Popper oxynitride.

Although layer perovskite oxynitrides containing divalent ions in the interlayer galleries have been reported [31–33], there are so far no examples of compounds that contain exchangeable cations. To our knowledge there are also no examples of perovskite oxynitrides prepared by a topochemical reaction. Here, we report the synthesis of a two- and three-layer Ruddlesden–Popper phase oxynitrides, from the previously known Dion–Jacobson phase photocatalysts $RbLaNb_2O_7$ and $RbCa_2Nb_3O_{10}$ [20]. We find that the conversion of the Dion–Jacobson phase oxides into Ruddlesden–Popper phase oxynitrides is indeed possible according to the reaction shown in Fig. 1. Although the resulting materials do absorb visible light, they are poor photocatalysts because they are unstable in aqueous media.

2. Synthesis

$RbCa_2Nb_3O_{10}$ was prepared by solid state reaction of Rb_2CO_3 (Aldrich 99.8%), $CaCO_3$ (Aldrich 99.995%), and Nb_2O_5 (Aldrich 99.99%). A 40% stoichiometric excess of Rb_2CO_3 was added to compensate for volatilization. Samples were ground, heated to 850 °C for 1 h to decompose the carbonates, then heated to 1100 °C for 12 h. $RbLaNb_2O_7$ was prepared from Rb_2CO_3 (Aldrich 99.8%), La_2O_3 (Aldrich 99.999%), and Nb_2O_5 (Aldrich 99.99%). La_2O_3 was dried at 1100 °C for 12 h prior to use. A 40% excess of Rb_2CO_3 was used to compensate for volatilization. The ground powder was heated to 850 °C for 1 h then heated to 1100 °C for 12 h. The phase purity of the products was determined by X-ray powder diffraction (XRD), by checking the powder patterns against prior literature reports [17,34].

Oxynitrides were synthesized from the appropriate precursor oxide, which was ground with a 40% stoichiometric excess of Rb_2CO_3 to compensate for volatilization. Samples were placed in a Ni boat and sealed in a resealable Ni alloy tube with removable gas tight valves attached to the ends. NH_3 (MG 99.99% or Aldrich 10% ^{15}N) gas was flowed through the tube for 30 min to displace air. The samples were then placed in a tube furnace, heated to 800 °C and held for 30 min under constant NH_3 flow of approximately 60 sccm. After cooling, argon was flowed through the tube to displace ammonia. Samples were unsealed from tube in an Ar atmosphere glove box where they were stored prior to characterization.

3. Instrumentation

Thermogravimetric analysis (TGA) was performed on a TA Instruments 2050 with minimal prior exposure to air. Data were collected under anhydrous air and nitrogen at scan rates of 5–10 °C/min. Solid state ^{15}N nuclear magnetic resonance (NMR) was performed using magic angle spinning (MAS) on a Chemagnetics CMX Infinity 500 Solid State NMR. The spectral frequency was 499.62 MHz, the spin rate was 6 kHz, and the pulse delay was 3.00 s. Initial X-ray diffraction (XRD) patterns were obtained on a Phillips X-Pert MPD diffractometer using monochromatized Cu$K\alpha$ ($\lambda = 1.5418$ Å) radiation. Scans were done in $\theta-\theta$ geometry, with samples held on a quartz zero-background plate under ambient conditions. For structure refinement, XRD patterns of samples in sealed quartz capillaries were obtained on beam line X3B1 of the National Synchrotron Light Source at Brookhaven National Laboratory. A wavelength of 0.8210 Å was selected by a Si(111) double crystal monochromator. Incident beam intensity was monitored by an ion chamber and used to normalize the signal. Rietveld structural refinement was done by using the GSAS [35,36] software package. Elemental nitrogen analysis was performed by Atlantic Microlabs, Inc. by combustion analysis on a sample packed under an Ar atmosphere. Energy-dispersive X-ray spectroscopy (EDS) was obtained from a JEOL-JSM 5400 scanning electron microscope from an average of three acquisitions. Inductively coupled plasma-mass spectrometry (ICP-MS) was performed on a Leeman Labs PS3000UV spectrophotometer, with acidified aqueous RbF standards on a sample dissolved in 48% HF. Oxygen composition was determined by difference. X-ray photoelectron spectroscopy (XPS) was done on a Kratos Analytical Axis Ultra photoelectron spectrometer using Al$K\alpha$ radiation with an approximate sampling depth of 25 Å on a sample exposed to the atmosphere only during sample mounting. Diffuse reflectance UV-Vis spectroscopy was done on a Perkin Elmer Lambda 900 UV-Vis spectrometer on pressed pellet samples referenced to a barium sulfate standard. Oxygen and hydrogen evolution experiments were performed in 10 mL of 0.01 M aqueous $AgNO_3$ or 10% methanol, respectively, as sacrificial acceptor and donor. Samples were typically purged in argon for 45 min, sealed, placed under an external flow of argon, then illuminated with a 400 W Xe/Hg lamp, with and without 380 nm pass filter. Headspace gas samples of 0.5 mL were removed from the sealed inner tube and injected into Varian 90-P3 gas chromatograph with a room-temperature molecular sieve 5A column and thermal conductivity detector. An Ophir Optronics photopower meter was used to determine the total absorbed incident radiation of the oxide and oxynitride. A single wavelength for the lamp was assumed from a weighted average of total output (843 nm), and recalculated for filtered radiation (980 nm).

4. Results and discussion

Reaction of the white three- and two-layer Dion–Jacobson oxide precursors with Rb_2CO_3 and gaseous ammonia at 800 °C gave bright yellow products. Preliminary analysis by XRD showed that the samples changed rapidly when exposed to air; thereafter, all products were transferred without exposure to air to an Ar atmosphere box, and care was taken to minimize contact with air or moisture in each type of analysis.

XPS was performed on the three-layer oxynitride product to determine if it was moisture or oxygen sensitive. Samples exposed for 3 h to anhydrous air or to water both showed a dramatic decrease in the surface nitrogen content, to 1.9 and 1.3 atom%, respectively, compared to a sample stored under argon, 11.6 atom% N (Table 1). Consistent with this observation, the oxygen to nitrogen ratios of both samples increased from 2.6 in the sample stored under argon to 24.2 and 41.2 for the oxygen- and water-exposed samples, respectively, due to surface hydrolysis and/or oxidation. Aluminum observed was presumed to be from the alumina crucibles used to synthesize the parent oxide.

Nitrogen-15 MAS NMR spectra were acquired in order to gain insight into the chemical state of nitrogen

Table 1
XPS surface composition data for $Rb_{1.8}Ca_2Nb_3O_{9.2}N_{0.8} \cdot 0.6H_2O$ after exposure to different atmospheres

Atmosphere	O	N	Ca	C	Nb	Rb	Al
Argon (atomic %)	29.6	11.6	4.9	27.6	5.1	20.3	0.8
Argon (mol ratio)[a]	2.6	1.0	0.4	—	0.4	1.7	—
Argon & water (atomic %)	53.6	1.3	10.5	11.6	11.7	10.5	0.7
Argon & water (mol ratio)[a]	41.2	1.0	8.1	—	9.0	8.1	—
Anhydrous air (atomic %)	45.9	1.9	5.7	26.5	6.8	10.9	2.3
Anhydrous air (mol ratio)[a]	24.2	1.0	3.0	—	3.6	5.7	—

[a]Mol ratios normalized to 1 mol N. C and Al excluded from mol ratio calculations.

in these compounds. The three-layer oxynitride gave a chemical shift of 84.8 ppm relative to CH_3NO_3 (Fig. 2). No signal in the region of the chemical shift of ammonia (380.23 ppm relative to nitromethane) was observed, indicating that nitrogen is coordinated within the perovskite blocks, and is not intercalated as ammonia in the interlayer galleries. Oxynitride ceramics and glasses have lower chemical shifts, typically between −200 and −300 ppm [37]. The relatively short pulse delay (3.00 s) used in our experiments may not have allowed for some nuclei in the perovskite blocks to relax. T_1 times of up to 3000 s have been observed in some ^{15}N MAS NMR experiments [37]. It is possible that the signal observed was due to only the defect sites in the system, and longer pulse delays could reveal different chemical shifts corresponding to lattice nitride.

Nitrogen combustion analysis for $Rb_{1.8}Ca_2Nb_3O_{9.2}N_{0.8}\cdot 0.6H_2O$ gave slightly less than the 2.00%w nitrogen expected on the basis of complete conversion (to $Rb_2Ca_2Nb_3O_9N\cdot 0.6H_2O$). The observed 1.67 ± 0.3%w gives 0.84 ± 0.15 mol of nitrogen per formula unit. Similarly the two-layer oxynitride gave only 0.73 ± 0.13 mol of nitrogen per formula unit. The lower than expected nitrogen content might be partially due to surface hydrolysis prior to the analysis from exposure to the air. The observation of lattice water in both compounds is consistent with this idea.

EDS analysis was used to estimate the ratio of Rb to other metallic elements (La, Ca, Nb) in the precursor oxides and product oxynitrides. The Rb *K* line in each of the oxides, $RbLaNb_2O_7$ and $RbCa_2Nb_3O_{10}$ was normalized to one. The corresponding oxynitrides gave Rb molar contents of 1.7 ± 0.2 and 2.1 ± 0.2 mol for the two- and three-layer phases, respectively. These are close to the predicted values of two Rb per formula unit for Ruddlesden–Popper phases. Excess rubidium appeared to volatilize during synthesis.

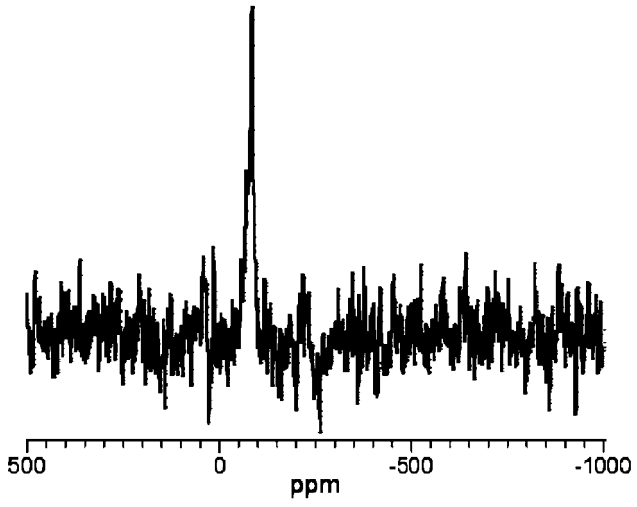

Fig. 2. ^{15}N-MAS NMR spectrum of $Rb_{1.8}Ca_2Nb_3O_{9.2}N_{0.8}\cdot 0.6H_2O$.

TGA of the oxynitrides showed a weight loss that was complete by about 250 °C. Coupling the TGA with MS showed that the weight loss in that region was solely due to water (Fig. 3). To check for possible ammonia loss, the $m/z = 17$ signal was monitored, but it was not distinguishable from noise and did not change in the regions where mass changes were observed. The weight gain seen at 590 °C correlates to oxidation of the oxynitride to the parent oxide with 0.8 mol excess rubidium, which then begins to volatilize. The $n = 2$ phase displayed similar TGAs. Because the ammonialysis reaction was done at much higher temperature (800 °C), the most likely source of this water is post-synthesis intercalation of water from purge gases or air. Dion–Jacobson and Ruddlesden–Popper phases are known to readily hydrate [38–41]. Assuming that no nitrogen was lost in heating up to 250 °C, the number of moles of water lost was 0.5–1.0 per formula unit for both the two- and three-layer oxynitrides.

Table 2 summarizes the water, nitrogen, and rubidium content of samples obtained by combining the TGA, combustion analysis, and ICP-MS results. There was some variability in the composition, for replicate samples. The amount of nitrogen determined by combustion analysis was consistent, varying between 0.84 and 0.66 mols for all samples. The rubidium analysis varied between 1.36 and 1.94 atoms for formula unit. The average (1.69) was the same as the amount (1.73) needed to charge compensate the nitrogen (average 0.73 atoms/formula unit), within experimental error, assuming that all the nitrogen is incorporated into

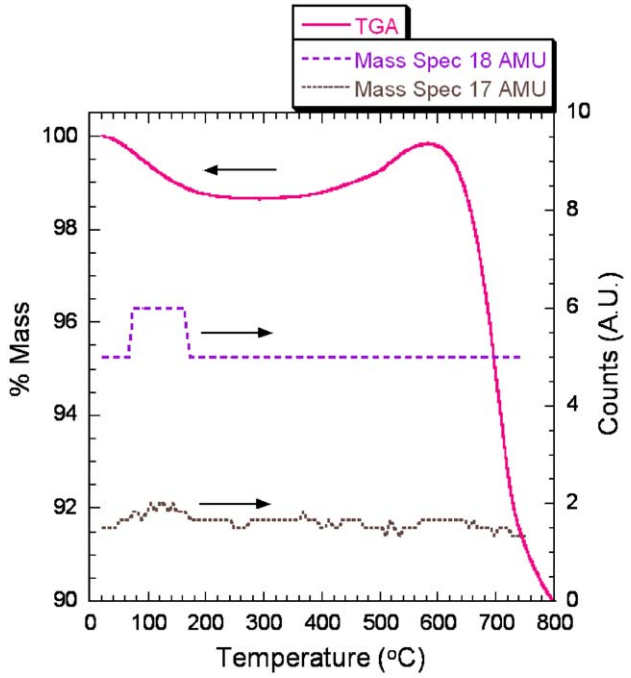

Fig. 3. TGA-MS of $Rb_{1.8}Ca_2Nb_3O_{9.2}N_{0.8}\cdot 0.6H_2O$.

Table 2
Water, nitrogen, and rubidium content (per formula unit) of several samples of two-layer ($n = 2$) and three-layer ($n = 3$) oxynitride Ruddlesden–Popper phases

	Mols water[a]	Mols nitrogen[b]	Mols rubidium[c]
$n = 2$	0.60±0.01	0.73±0.13	1.74±0.10
$n = 2$	1.05±0.01	0.72±0.13	1.94±0.10
$n = 2$	1.01±0.01	0.70±0.13	1.81±0.10
$n = 2$	0.54±0.01	0.66±0.13	1.47±0.10
$n = 3$	0.62±0.01	0.84±0.14	1.79±0.10
$n = 3$	0.47±0.01	0.74±0.14	1.72±0.10
$n = 3$	0.44±0.01	0.74±0.14	1.36±0.10

[a]Moles of water determined by TGA, error calculated from error in Nitrogen and Rubidium.
[b]Moles of nitrogen determined by elemental combustion analysis, error reported by Atlantic Microlabs Inc.
[c]Moles of Rubidium determined by ICP-MS, error determined from standard deviation.

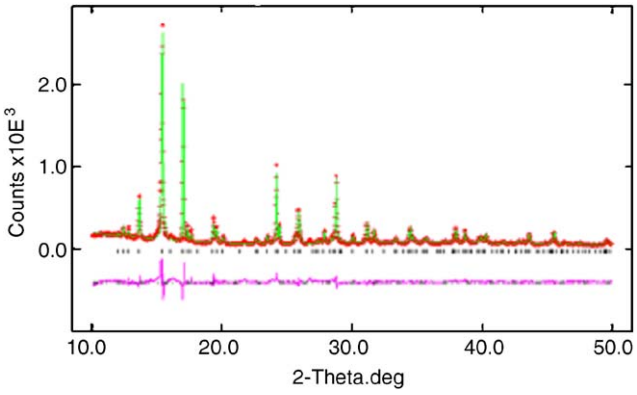

Fig. 4. GSAS refinement of synchrotron X-ray powder diffraction pattern of $Rb_{1.8}LaNb_2O_{6.3}N_{0.7} \cdot 1.0H_2O$ showing observed (top solid line) and calculated (top crosses) intensities, difference (bottom solid line) and allowed Bragg reflections (tick marks).

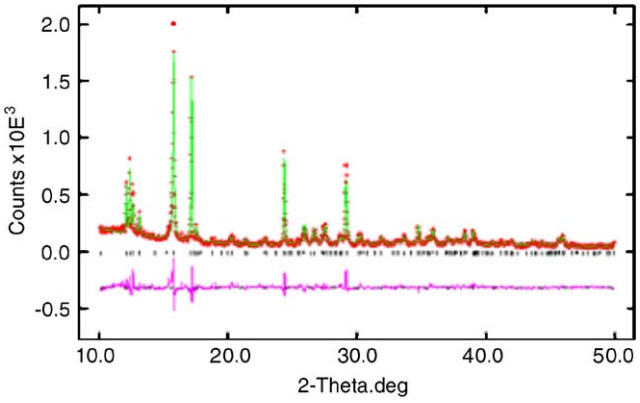

Fig. 5. GSAS refinement of X-ray powder diffraction data for $Rb_{1.7}Ca_2Nb_3O_{9.3}N_{0.7} \cdot 0.5H_2O$ showing observed (top solid line) and calculated (top crosses) intensities, difference (bottom solid line) and allowed Bragg reflections (tick marks).

anion sites in the lattice. The water content showed the most variability between samples, as might be expected for intercalated water. In all but one sample the rubidium is present in the appropriate amount to charge compensate the incorporation of nitrogen, within experimental error.

Synchrotron XRD data were obtained for two- and three-layer samples with analytical compositions $Rb_{1.8}LaNb_2O_{6.3}N_{0.7} \cdot 1.0H_2O$ and $Rb_{1.7}Ca_2Nb_3O_{9.3}N_{0.7} \cdot 0.5H_2O$. Care was taken to avoid exposure to air prior to data acquisition. The typical body centered ($I4/mmm$) structure that is adopted by many Ruddlesden–Popper oxides failed to give reasonable fits for these compounds. Superlattice ($a\sqrt{2}$) structures with tilting of the NbO_6 octahedra were investigated, and these models also gave poor fits.

Ruddlesden–Popper phases have been found to form hydrated structures in which the layers shift to an eclipsed arrangement in a primitive tetragonal unit cell [38]. Therefore primitive models were constructed and both structures were refined in space group $P4/mmm$. Refinement of the two- and three-layer oxynitride patterns in this space group gave cell parameters $a = 3.934(2)$ and $c = 14.679(2)$ Å for $n = 2$, and $a = 3.887(3)$ and $c = 18.65(1)$ for $n = 3$ (Figs. 4 and 5, respectively). The nitrogen atoms were assumed to be evenly distributed over all lattice anion sites, although recent studies suggest that the anions are ordered in some oxynitrides [32,33] and oxyfluoride [42] perovskites. Additionally, all the O^{-2}/N^{-3} sites were refined as oxygen atoms.

The two- and three-layer oxynitrides structures were first refined without inclusion of water. Fourier difference maps were then used to determine the position of the water oxygen atoms. These atoms were then placed in the cell and the refinement was continued. In the two-layer compound, the water oxygen atom was placed at Wyckoff position 1*b* (0, 0, 1/2) (Table 3) as suggested by the Fourier difference map. This gave a better fit than oxygen at (1/2, 0, 1/2), or floated at a general position between the rubidium cations. Floated oxygens placed at Wyckoff positions 8*r* and 2*g* were shifted to (0, 0, 1/2) by the structural refinement. The final weighted-profile R value (R_{wp}) was 11.22% for the two-layer compound. In the refinement of the three-layer structure, the water oxygen atom was allowed to float at Wyckoff position 2*g* and settled at (0, 0, 0.444(2)) (Table 4). Placing the oxygen at general position 2*g* gave a better fit than the special position found for the two-layer compound. The R_{wp} was calculated to be 11.16%. Some weak reflections corresponding to a three-dimensional perovskite impurity phase were observed in both XRD patterns.

Bond lengths found for the oxynitrides (Table 5) are consistent within the perovskite block for two- and

Table 3
Factional coordinates, lattice parameters, and fitting parameters for $Rb_{1.8}LaNb_2O_{6.3}N_{0.7}\cdot 1.0H_2O$

Atom	Wyckoff posn	Frac	x	y	z	U_{iso}
O1/N1	1*a*	0.85(7)	0	0	0	0.006(2)
La1	1*c*	0.93(3)	0.5	0.5	0	0.0010(1)
Nb1	2*g*	0.93(4)	0	0	0.1518(3)	0.0010(2)
O2/N2	4*i*	1.00(4)	0.5	0	0.126(1)	0.0038(8)
O3/N3	2*g*	0.70(4)	0	0	0.283(2)	0.0003(8)
Rb1	2*h*	0.82(1)	0.5	0.5	0.3460(3)	0.0042(2)
Ow	1*b*	1.2(5)	0	0	0.5	0.023(3)

Lattice parameters $a = 3.934(2)$ and $c = 14.697(2)$ Å. Space group $P4/mmm$. $R_{wp} = 11.16\%$, $R_p = 8.62\%$, $\chi^2 = 4.490$.

Table 4
Factional coordinates, lattice parameters, and fitting parameters for $Rb_{1.7}Ca_2Nb_3O_{9.3}N_{0.7}\cdot 0.5H_2O$

Atom	Wyckoff posn	Frac	x	y	z	U_{iso}
Nb1	1*a*	0.87(2)	0	0	0	0.0008(3)
O1/N1	2*f*	1.3(2)	0.5	0	0	0.010(3)
O2/N2	2*g*	1.3(1)	0	0	0.894(4)	0.025(4)
Ca1	2*h*	0.94(3)	0.5	0.5	0.1126 (8)	0.0026(4)
Nb2	2*g*	0.76(1)	0	0	0.2268(3)	−0.0001(2)
O3/N3	4*i*	1.12(7)	0.5	0	0.212(1)	0.007(2)
O4/N4	2*g*	1.07(8)	0	0	0.318(2)	0.007(2)
Rb1	2*h*	0.69(1)	0.5	0.5	0.3823(6)	0.0042(3)
Ow	2*g*	0.73(6)	0	0	0.444(2)	0.005(2)

Lattice parameters $a = 3.887(3)$ and $c = 18.65(1)$ Å. Space group $P4/mmm$. $R_{wp} = 10.95\%$, $R_p = 8.62\%$ $\chi^2 = 4.370$.

Table 5
Selected bond lengths (Å) for oxynitride layer perovskites

$Rb_{1.8}LaNb_2O_{6.3}N_{0.7}\cdot 1.0H_2O$		$Rb_{1.7}Ca_2Nb_3O_{9.3}N_{0.7}\cdot 0.5H_2O$	
Nb1–O1	2.241(5)	Nb1-O1 (× 4)	1.9436(14)
Nb1–O2 (× 4)	1.998(4)	Nb1–O2 (× 2)	1.83(5)
Nb1–O3	1.601(23)	Nb2–O2	2.36(5)
		Nb2–O3 (× 4)	1.980(5)
		Nb2–O4	1.49(5)

three-layer oxide perovskites [17,34,38,43]. The NbO_6 octahedra in $Rb_{1.8}LaNb_2O_{6.3}N_{0.7}\cdot 1.0H_2O$ displays a distortion in the axial direction with bond lengths of Nb1–O1 = 2.241(5) Å and Nb1–O3 = 1.601(23) Å, as seen in Fig. 6a. There is a shortening of O–Nb–O bond length by about 0.1 Å compared to the parent oxide [17]. Shortening of the terminal Nb–O bonds in the three-layer perovskite blocks is also seen in Fig. 6b for $Rb_{1.7}Ca_2Nb_3O_{9.3}N_{0.7}\cdot 0.5H_2O$ (Nb2–O4 = 1.49(5) Å and Nb2–O2 = 2.36(5) Å). The terminal octahedra are shortened by about 0.2 Å when compared to Dion–Jacobson oxides of similar composition [34]. Bond lengths in the equatorial direction exhibit little variation from the parent oxide phases for either the two- or three-layer compounds.

UV-Vis diffuse reflectance (Fig. 7) confirmed that the band gap energies (E_g) of the bright yellow oxynitrides are in the visible region, i.e., shifted to lower energies relative to the parent oxide materials. The Kubelka–Munk function [$F(R)$], which can be expressed as the ratio of the absorption coefficient (K) to the scattering coefficient (S), was calculated from the diffuse reflectance (R) according to Eq. (1) [44].

$$F(R) = \frac{K}{S} = \frac{(R-1)^2}{2R}. \quad (1)$$

The type of band gap can be determined from plots of K^m vs energy ($h\nu$), where $m = 2$ or $1/2$. Samples with a direct band gap will have a linear region when K^2 vs energy is plotted, while indirect band gaps will be have a linear region when $K^{1/2}$ vs energy is plotted (Eq. (2)).

$$K^m = h\nu - E_g (m = \tfrac{1}{2} \text{ or } 2) \quad (2)$$

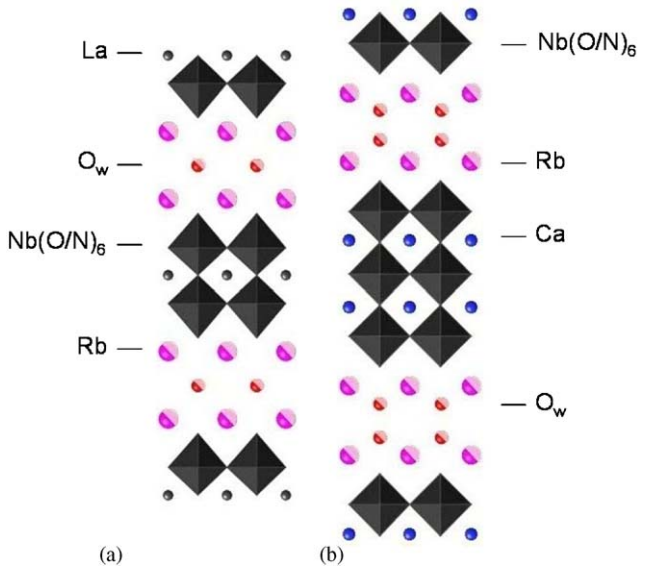

Fig. 6. Crystal structures of (a) $Rb_{1.8}LaNb_2O_{6.3}N_{0.7}\cdot 1.0H_2O$ and (b) $Rb_{1.7}Ca_2Nb_3O_{9.3}N_{0.7}\cdot 0.5H_2O$, showing fractional occupancy of interlayer Rb and lattice water oxygen atoms.

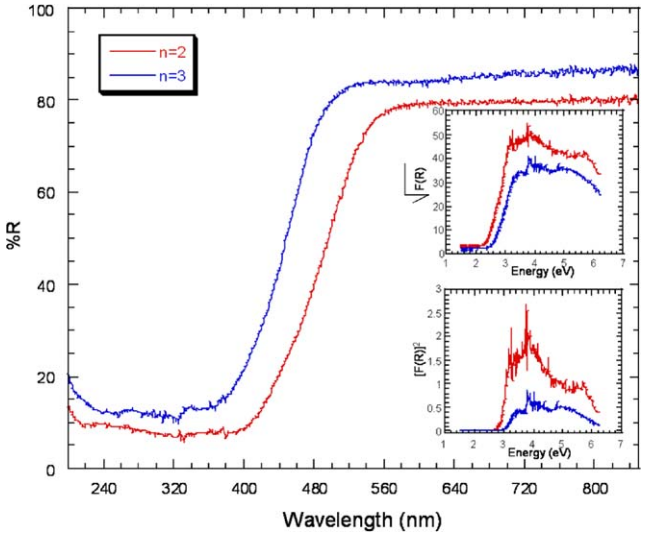

Fig. 7. Diffuse reflectance UV-visible spectra of $Rb_{1.7}LaNb_2O_{6.3}N_{0.7}\cdot 0.6H_2O$ ($n=2$) and $Rb_{1.8}Ca_2Nb_3O_{9.2}N_{0.8}\cdot 0.6H_2O$ ($n=3$). Plot of square root of the Kubelka–Munk function vs energy (inset a) and the Kubelka–Munk function squared vs energy (inset b).

E_g can be determined in either case from the energy intercept of the extrapolated linear portion of the graph. Similarly, one can plot $F(R)$ vs energy to determine the type of band gap. An indirect band gap plot for $Rb_{1.7}LaNb_2O_{6.3}N_{0.7}\cdot 0.6H_2O$ gives an E_g value of 2.29 eV. The same plot for $Rb_{1.8}Ca_2Nb_3O_{9.2}N_{0.8}\cdot 0.6H_2O$ gives an E_g value of 2.51 eV (Fig. 7a). There is also evidence for direct band gap transitions occurring at higher energies for the $n=2$ and 3 oxynitrides, at 2.84 and 2.99 eV, respectively (Fig. 7b).

Photocatalytic water decomposition was studied by comparing the three-layer oxynitride to the precursor Dion–Jacobson phase oxide $RbCa_2Nb_3O_{10}$. Hydrogen and oxygen evolution reactions were probed separately using sacrificial donors or acceptors shown in Scheme 1.

Experiments performed with light from an unfiltered Xe lamp source (containing both UV and visible light) show a clear trend of oxygen and hydrogen evolution for both materials (Fig. 8a). Oxygen evolution of the oxide was not as efficient as previously reported [20] due to the differences in the apparatus used to make the measurements. Domen and co-workers found an oxygen

$$4Ag^{+}_{(aq)} + 2H_2O_{(l)} \rightarrow 4Ag_{(s)} + O_{2(g)} + H^{+}_{(aq)} \qquad E^0 = -0.431\ V$$

$$CH_3OH_{(l)} + H_2O_{(l)} \rightarrow 3H_{2(g)} + CO_{2(g)} \qquad E^0 = -0.2\ V$$

Scheme 1. Oxygen and hydrogen evolution reactions.

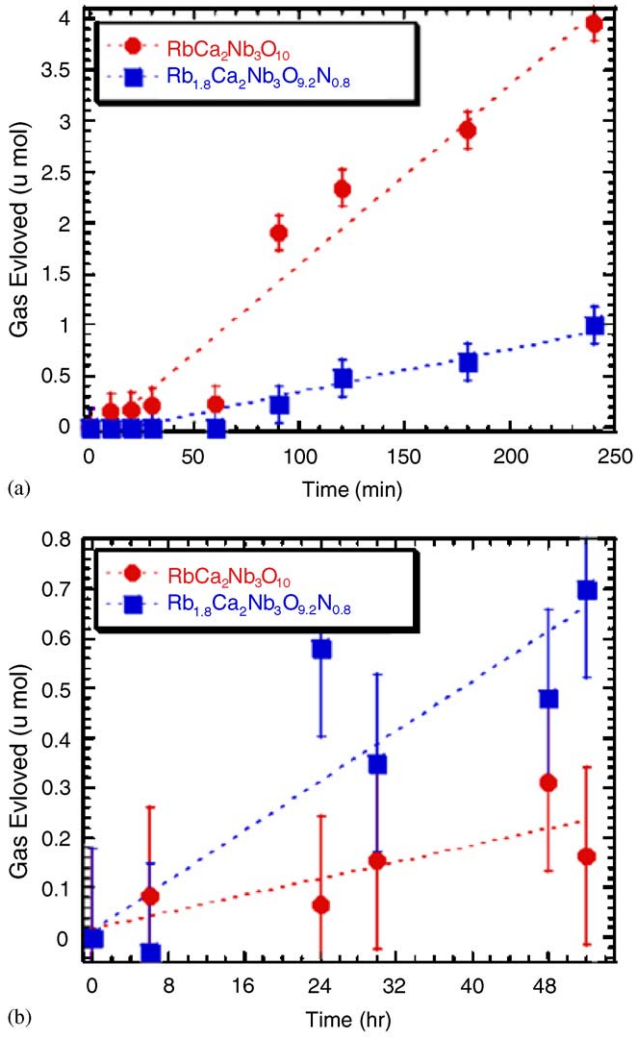

Fig. 8. Oxygen evolution vs. time for $RbCa_2Nb_3O_{10}$ (●) and $Rb_{1.8}Ca_2Nb_3O_{9.2}N_{0.8}\cdot 0.6H_2O$ (■) with an unfiltered xenon lamp (a) and with 380 nm pass filter (b).

Table 6
Quantum yields and oxygen evolution rates of the oxide and oxynitride under a filter and unfiltered Xe lamp source

Sample	Source	O_2 evolution rate (μmol/h)	Quantum yield (%)
$RbCa_2Nb_3O_{10}$	Unfiltered Xe lamp	1.180	1.052
$Rb_{1.8}Ca_2Nb_3O_{9.2}N_{0.8} \cdot 0.6H_2O$	Unfiltered Xe lamp	0.495	0.699
$Rb_{1.8}Ca_2Nb_3O_{9.2}N_{0.8} \cdot 0.6H_2O$	380 nm pass filter	0.021	0.025
$RbCa_2Nb_3O_{10}$	380 nm pass filter	0.006	0.008

evolution rate of 16 μmol/h, using an immersion method to irradiate their samples, compared to 1.2 μmol/h observed here using an external collimated light source to illuminate one face of a quartz reactor. QY were calculated using Eq. (3), in which A is the number of electrons transferred in the photoreaction (four in the case of O_2 evolution), R is the rate of gas evolution, and I is the rate at which photons are absorbed by the material.

$$QY = AR/I \times 100. \quad (3)$$

The Dion–Jacobson oxide $RbCa_2Nb_3O_{10}$ is a better photocatalyst under UV-Vis conditions with a QY of 1.05%, relative to the oxynitride which had a QY of 0.70% (Table 6). Because the oxynitride is unstable in contact with water (see Table 1), it is likely that an oxide product forms on the surface of the material, and this reduces the QY. Nitrogen detected by GC was typically 10 mol% of the oxygen evolved when the samples were illuminated with unfiltered UV-visible light, and was 30 mol% when 380 nm filtered light was used. Although oxynitrides under similar conditions have been reported to evolve nitrogen [30,45], the observed nitrogen could also arise from atmospheric nitrogen (and oxygen) leaking into the cell. A dark control experiment showed a nitrogen evolution rate of 0.052 μmol/h, accounting for essentially all of the N_2 observed, and this background leak rate was used to correct the amount of oxygen detected.

Oxygen evolution under 380 nm pass filter was greatly reduced compared to that observed using unfiltered light (Fig. 8b). The reduction in photocatalytic activity is expected for $RbCa_2Nb_3O_{10}$ because the filter blocks light with $E > E_g$. The oxynitride generated a small amount of oxygen (0.021 μmol/h) but more than oxide (0.006 μmol/h). This oxygen evolution rate corresponds to a QY for $Rb_{1.8}Ca_2Nb_3O_{9.2}N_{0.8} \cdot 0.6H_2O$ of 0.025%. This is significantly lower than that reported for the three-dimensional oxynitride perovskite $LaTiO_2N$ (1.5% QY) [30], with the difference attributable primarily to the instability of the layered oxynitride. Hydrogen evolution was not detected for either $RbCa_2Nb_3O_{10}$ or $Rb_{1.8}Ca_2Nb_3O_{9.2}N_{0.8} \cdot 0.6H_2O$ under filtered light.

5. Conclusions

Ammonialysis in the presence of Rb_2CO_3 converts the $RbCa_2Nb_3O_{10}$ Dion–Jacobson phase to a Ruddlesden–Popper oxynitride $Rb_{1.8}Ca_2Nb_3O_{9.2}N_{0.8} \cdot yH_2O$. The two-layer Dion–Jacobson oxide $RbLaNb_2O_7$ undergoes the same reaction to form $Rb_{1.8}LaNb_2O_{6.3}N_{0.7} \cdot yH_2O$. These materials have band gaps in the visible region, but because they are unstable in water, their photocatalytic activity is quite poor. Conversion of Dion–Jacobson oxides to Ruddlesden–Popper oxynitrides may be generalizable beyond these particular compounds, and other variants (e.g., those with higher interlayer charge) may be more resistant to air oxidation and hydrolysis. Such materials might also be of interest as oxynitride pigments [46] and dielectric materials [47] in anydrous environments.

Acknowledgments

This work was supported by the Division of Chemical Sciences, Office of Basic Energy Sciences, US Department of Energy under Contract DE-FG02-93ER14374.

References

[1] R.J. Cava, B. Batlogg, R.B. van Dover, D.W. Murphy, S. Sunshine, T. Siegrist, J.P. Remeika, E.A. Rietman, S. Zahurak, G.P. Espinosa, Phys. Rev. Lett. 58 (1987) 1676.
[2] K.D. Otzschi, K.R. Poeppelmeier, P.A. Salvador, T.O. Mason, H. Zhang, L.D. Marks, J. Am. Chem. Soc. 118 (1996) 8951.
[3] F. Galasso, W. Dardy, Inorg. Chem. 4 (1965) 71.
[4] Y. Moritomo, A. Asamitsu, H. Kuwahara, Y. Tokura, Nature 380 (1996) 141.
[5] K. Domen, A. Kudo, T. Onishi, J. Catal. 102 (1986) 92.
[6] K. Domen, A. Kudo, T. Onishi, N. Kosugi, K. Kuroda, J. Phys. Chem. 90 (1986) 292.
[7] A. Kudo, A. Tanaka, K. Domen, K. Maruya, K. Aika, T. Onishi, J. Catal. 111 (1988) 67.
[8] S. Uma, A.R. Raja, J. Gopalakrishnan, J. Mater. Chem. 3 (1993) 709.
[9] J. Gopalakrishnan, Chem. Mater. 7 (1995) 1265–1275.
[10] J. Gopalakrishnan, T. Sivakumar, K. Ramesha, V. Thangadurai, G.N. Subbanna, J. Am. Chem. Soc. 122 (2000) 6237–6241.
[11] R.E. Schaak, T.E. Mallouk, Chem. Mater. 14 (2002) 1455–1471.

[12] M. Dion, M. Ganne, M. Tournoux, Mater. Res. Bull. 16 (1981) 1429.
[13] M. Dion, M. Ganne, M. Tournoux, Rev. Chim. Mineral 21 (1984) 92.
[14] A.J. Jacobson, J.W. Johnson, J.T. Lewandowski, Inorg. Chem. 24 (1985) 3727.
[15] S.N. Ruddlesden, P. Popper, Acta Cryst. 10 (1957) 538.
[16] S.N. Ruddlesden, P. Popper, Acta Cryst. 11 (1958) 54.
[17] A.R. Armstrong, P.A. Anderson, Inorg. Chem. 33 (1994) 4366.
[18] H. Kato, A. Kudo, J. Phys. Chem. B 105 (2001) 4285.
[19] A. Fujishima, K. Honda, Nature 238 (1972) 37.
[20] K. Domen, J. Yoshimura, T. Sekine, A. Tanaka, T. Onishi, Catal. Lett. 4 (1990) 339.
[21] T. Takata, Y. Furumi, K. Shinohara, A. Tanaka, M. Hara, J.N. Kondo, K. Domen, Chem. Mater. 9 (1997) 1063.
[22] M. Machida, K. Miyazaki, S. Matsushima, M. Arai, J. Mater. Chem. 13 (2003) 1433–1437.
[23] R. Marchard, F. Pors, Y. Laurent, Ann. Chim. Fr. 16 (1991) 553.
[24] R. Marchard, F. Pors, Y. Laurent, Ann. Chim. Fr. 16 (1991) 547.
[25] E. Gunther, R. Hagenmayer, M. Jansen, Z. Anorg. Allg. Chem. 626 (2000) 1519.
[26] N. Diot, R. Marchard, J. Haines, J.M. Leger, P. Macaudiere, S. Hull, J. Solid State Chem. 146 (1999) 390.
[27] S.J. Clarke, B.P. Guinot, C.W. Michie, M.J.C. Calmont, M.J. Rosseinsky, Chem. Mater. 14 (2002) 288–294.
[28] G. Hitoki, T. Takata, J.N. Kondo, M. Hara, H. Kobayashi, K. Domen, Chem. Commun. (2002) 1698.
[29] G. Hitoki, A. Ishikawa, T. Takata, J.N. Kondo, M. Hara, K. Domen, Chem. Lett. 7 (2002) 736.
[30] A. Kasahara, K. Nukumizu, T. Takata, J.N. Kondo, M. Hara, H. Kobayashi, K. Domen, J. Phys. Chem. B 107 (2003) 791.
[31] G. Tobias, J. Oro-Sole, D. Beltran-Porter, A. Fuertes, Inorg. Chem. 40 (2001) 6867.
[32] G. Tobias, D. Beltran-Porter, O.I. Lebedev, G. Van Tendeloo, J. Rodriguez-Carvajal, A. Fuertes, Inorg. Chem. 43 (2004) 8010.
[33] S.J. Clarke, K.A. Hardstone, C.W. Michie, M.J. Rosseinsky, Chem. Mater. 14 (2002) 2664.
[34] V. Thangadurai, P. Schmid-Beurmann, W. Weppner, J. Solid State Chem. 158 (2001) 279.
[35] ACLaRBV Dreele, General Structure Analysis System (GSAS), Los Alamos National Laboratory Report LAUR 86-748, 2000.
[36] B.H. Toby, EXPGUI, J. Appl. Cryst. (2001) 210–213.
[37] K.J.D. Mackenzie, M.E. Smith, Multinuclear Solid-State NMR or Inorganic Materials, Elsevier Science Ltd., Oxford, 2002.
[38] T.A. Kodenkandath, J.B. Wiley, Mater. Res. Bull. 35 (2000) 1737.
[39] M. Sato, J. Abo, T. Jin, Solid State Ion. 57 (1992) 285–293.
[40] R.E. Schaak, T.E. Mallouk, J. Solid State Chem. 155 (2000) 46.
[41] R.E. Schaak, T.E. Mallouk, J. Solid State Chem. 161 (2001) 225–232.
[42] J.H. Choy, J.Y. Kim, S.J. Kim, J.S. Sohn, Chem. Mater. 13 (2001) 906.
[43] S.H. Byeon, S.O. Lee, H. Kim, J. Solid State Chem. 130 (1997) 110.
[44] P. Kubelka, F. Munk, Z. Tech. Phys. 12 (1931) 593.
[45] A. Kasahara, K. Nukumizu, G. Hitoki, T. Takata, J.N. Kondo, M. Hara, H. Kobayashi, K. Domen, J. Phys. Chem. A 106 (2002) 6750.
[46] M. Jansen, H.P. Letschert, Nature 404 (2000) 980.
[47] Y.I. Kim, P.M. Woodward, K.Z. Baba-Kishi, C.W. Tai, Chem. Mater. 16 (2004) 1267.